

Multi-dimensional magnetic resonance imaging in a stray magnetic field

Jay H. Baltisberger^{a,*}, Sabine Hediger^b, Lyndon Emsley^b

^a Department of Chemistry, Berea College, Berea, KY 40404, United States

^b Laboratoire de Chimie (UMR 5182 CNRS/ENS), Laboratoire de Recherche Conventionné du CEA (23V), Ecole Normale Supérieure de Lyon, 69364 Lyon, France

Received 1 July 2004

Abstract

Stray field imaging has been extensively utilized in the last 10 years to perform very high resolution imaging of samples in a single dimension using the massive field gradient present in the fringe of a superconducting magnet. By spinning the sample around the magic-angle, the stray field gradient is successively reoriented along three orthogonal directions in the sample reference frame, allowing the acquisition of a full three-dimensional Fourier image, thereby providing the possibility to perform multi-dimensional very high-resolution imaging with standard nuclear magnetic resonance spectroscopy equipment. Here, we show multi-dimensional images demonstrating the feasibility of this technique.

© 2004 Elsevier Inc. All rights reserved.

Keywords: Stray field imaging; MRI; Magic-angle spinning; Inhomogeneous magnetic fields; Spatial resolution

1. Introduction

The basic theory of magnetic resonance imaging (MRI) was discovered by Lauterbur and Mansfield in 1973 [1,2] and involves rendering the NMR frequency of H₂O (or another material) dependent on the spatial location by applying a magnetic field gradient across the sample. This mapping of spatial locations to specific frequencies can be used to generate a three-dimensional density profile of a sample [3], and is the foundation of all MRI experiments used today. In conventional MRI, field gradients are generated by different coils supplementary to the main solenoid which are turned on and off in each direction as appropriate. Spatial resolution in MRI is determined by the strength of the gradient.

The stronger the gradient, the better the resolution can be. To improve the spatial resolution of MRI, Samoilenko [4] proposed in 1988 the stray field magnetic resonance imaging (STRAFI) experiment, which takes advantage of the very large *z*-gradient present in the static magnetic field of a superconducting NMR magnet [4–8]. This fixed gradient (10–100 T/m) is much larger than any that can be generated using conventional pulsed field gradient approaches and has the possibility of affording the greatest spatial resolution. With a gradient of 75 T/m and a proton linewidth of 1 Hz, the spatial resolution could theoretically approach 30 nm. The fundamental problem with STRAFI is the one-dimensional nature of the experiment. Since the gradient of the fixed *B*₀ field is used, imaging information can only be collected along the fixed axis of the stray field (say *z*). It was already proposed to use additional pulsed field gradients in the other two dimensions and have thus a mixed resolution experiment, high in the *z*-direction, and low along the *x*- and *y*-axis [9]. It would however

* Corresponding author. Fax: +1 859 985 3303.

E-mail addresses: jay_baltisberger@bera.edu (J.H. Baltisberger), sabine.hediger@ens-lyon.fr (S. Hediger), lyndon.emsley@ens-lyon.fr (L. Emsley).

be better to use the fixed stray field gradient to image all three dimensions. In this sense, a probe has been patented which mechanically reorients the sample along two different axes, both orthogonal to the z -direction [10]. The three-dimensional image is reconstructed by back-projection reconstruction techniques from a set of one-dimensional profiles measured point-by-point for each position of the sample in the stray field [11], similar to the projection reconstruction approach to imaging where the gradient changes direction. This approach is however time-consuming and requires very specialized equipment [9–12]. For these reasons the number of applications in the literature has kept limited [11–14].

Here, we show how by reorienting the z -gradient during the course of a multi-dimensional NMR experiment a complete Fourier image can be obtained. For that purpose, a continuous rotation of the sample at the so-called magic-angle is performed. Magic-angle sample spinning (MAS) is a technique routinely used in solid-state NMR which allows the averaging of second-rank tensor interactions [15,16]. The enormous advantage of this approach is that virtually every NMR laboratory now has the tools to do three-dimensional-STRAFI experiments using a conventional MAS probe and a superconducting NMR magnet. If the MAS rotor (or other rotating sample compartment) could be made smaller (the size of a capillary tube) and rotated slowly about the magic-angle, it is quite feasible that using a micro coil, the goal of sub-micron resolution might be achieved.

A schematic description of the way the stray field z -gradient is reoriented is given in Fig. 1. The sample rotation axis, called the magic-angle, forms an angle of 54.7° with the direction of the magnetic field (z -axis) and corresponds to the body diagonal of a cube. When the cube is rotated about its body diagonal, e.g., the magic angle, the three x , y , and z sample-fixed axes undergo a cyclic permutation after each one-third of a complete rotation (x becomes z becomes y becomes x). It follows that the static gradient, which is fixed along the z -axis of the laboratory frame, becomes successively aligned with the z -, y -, and x -axis of the sample frame during a complete 360° rotation of the sample. A three-dimensional proton

density profile of the sample can thus be obtained from the three-dimensional Fourier-transform experiment in which the protons in a sample are excited and then allowed to evolve successively at each of the three orientations described in Fig. 1 for incremented times t_1 , t_2 , and t_3 , respectively. The experiment can be modified to give either a two-dimensional projection of the sample by only using two of the three orientations, or a two-dimensional thin slice by using a frequency selective pulse at the initial orientation before evolving at the second, and third sample orientations.

The remaining question for the design of such experiments is how to turn off the evolution of the magnetization while the sample is rotating from one orientation to the next (which takes about 3 ms for a rotation rate of approximately 100 Hz). This problem is very close to the one found in the magic-angle hopping [17,18] or magic-angle turning (MAT) [19–21] NMR experiment, where a high-resolution spectrum in the solid-state is obtained by averaging the chemical shift measured after each one-third of the rotor period [17–21]. Basically, two solutions are possible to stop the evolution of the magnetization during the reorientation time. The first one is to use z -filters, pairs of 90° pulses which store the magnetization along the static magnetic field (z -axis of laboratory frame) during the reorientation of the sample, and recall it to the transverse plane once the sample is correctly repositioned. The original MAT experiment was built on this concept [19]. The second solution is to refocus the evolution of the spins during the reorientation of the sample using 180° refocusing pulses, as used in later modified MAT experiments [18,20]. The modified MAT experiment has the advantage of much higher sensitivity.

2. Results and discussion

Some possible pulse sequences for MAS-STRAFI are shown in Fig. 2. Figs. 2A and D are the sequences leading to a full three-dimensional image using z -filters or refocusing pulses, respectively. The sequence based on z -filters is much shorter than the “refocusing” version and may therefore be of advantage for samples with rel-

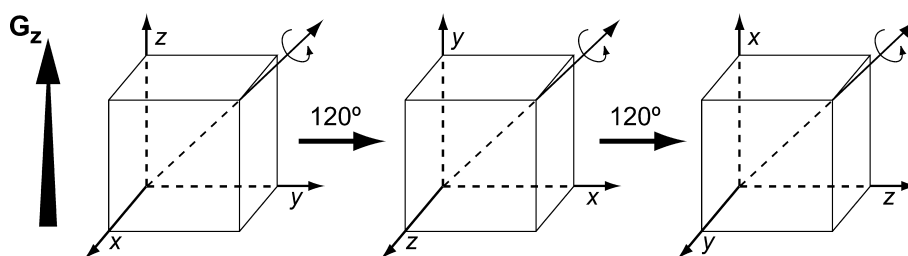


Fig. 1. Diagram showing a cube undergoing magic-angle spinning over two-thirds of a revolution. Notice that the sample axis aligned with the field gradient undergoes a cyclic permutation between x , y , and z after each one-third of a revolution.

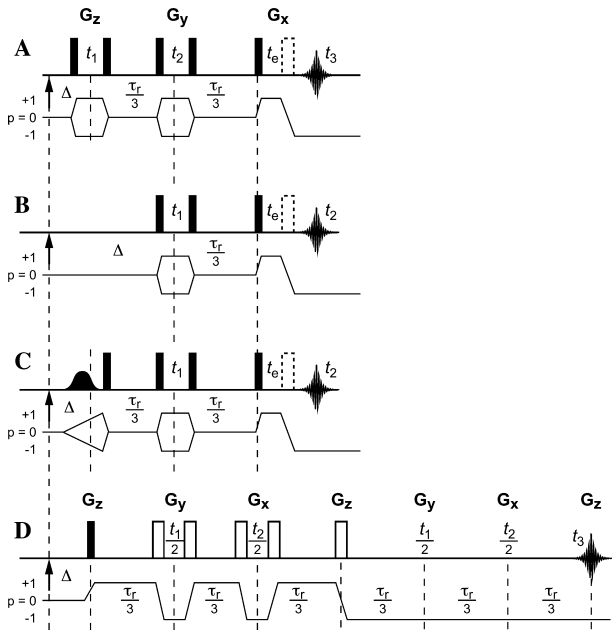


Fig. 2. Pulse sequences proposed to obtain multi-dimensional images using the MAS-STRAFI technique. Filled and open rectangles represent 90° and 180° pulses, respectively. A small arrow indicates the rotor-phase signal for active triggering of the start of the sequence. Vertical dashed bars indicate the rotor timing. They are spaced by one-third of a rotor period, $\tau_r/3$, which corresponds to the time needed to move the gradient between orthogonal directions in the sample frame of reference according to Fig. 1. The desired coherence pathway is drawn below each sequence. Phase cycling of the pulses has to be performed accordingly. The sequence in (A) and (D) lead to a full three-dimensional image, using either z -filters (A) or refocusing 180° pulses (D) to avoid signal evolution during the reorientation of the gradient in the sample frame of reference. Based on z -filters, sequence (B) will produce a two-dimensional projection image, and sequence (C) a two-dimensional slice through the object studied, done by replacing the first dimension with a slice selective pulse. For sequences (A)–(C), using an echo for detection will normally improve signal-to-noise as well as eliminate dead time issues. To keep the detection time t_3 at the correct orientation of the gradient with respect to the sample, the echo time should either be kept very small with the signal detection starting on the top of the echo, or set to one rotor period which allows a full echo acquisition but requires long T_2 relaxation times of the sample. Sequence (D) does not need any additional pulse to produce an echo in the detection dimension. Pulse sequences are available upon request to the authors.

atively short T_2 relaxation times. It also allows straightforward acquisition of an amplitude-modulated signal in both indirect detection times through the simultaneous detection of $+1$ and -1 -coherence pathways, avoiding thus distortions of the image by mixed phase signal components. In the sequence with z -filters, signal detection is started straight after the last 90° pulse. This can lead to distortions of the profile due to receiver dead-time problems. It is therefore recommended to perform an echo acquisition with an additional 180° refocusing pulse (shaded pulse). The sequence of Fig. 2D based on refocusing pulses directly produces an echo in the detection dimension. The sequences of Figs. 2B and C have been

derived from Fig. 2A. They can be used to obtain two-dimensional projections (2B) or slices (2C) of the sample using the z -filter technique. Analogous sequences based on the “refocusing” technique can be derived from Fig. 2D, but are not shown.

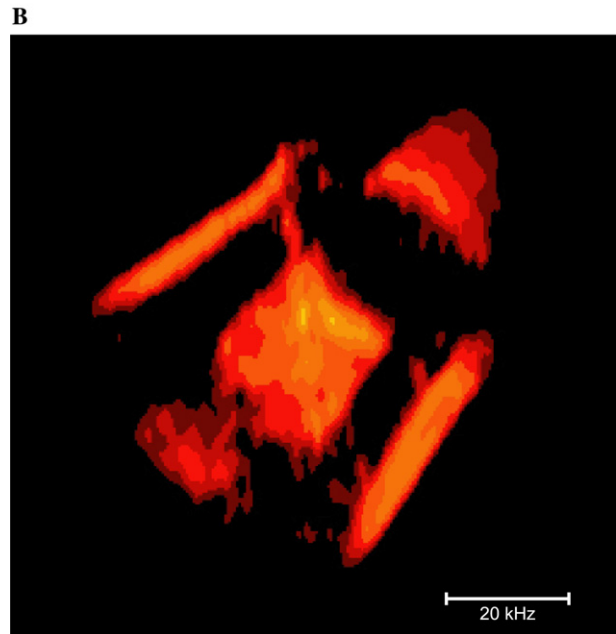
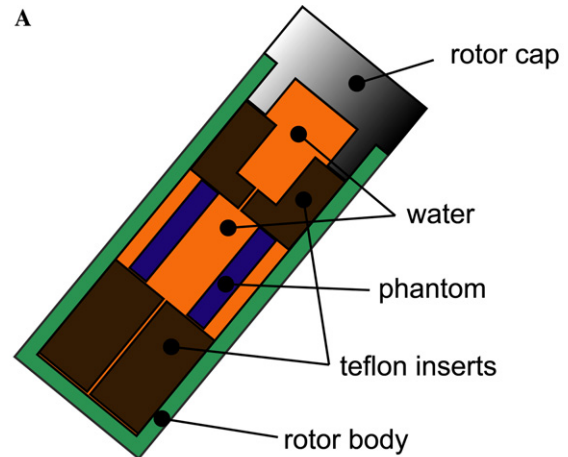


Fig. 3. (A) Geometry of the phantom object, a small plastic cylinder (2.84 mm height, 2.39 mm external diameter, and 1.32 mm internal diameter) placed in a standard 4 mm external-diameter MAS rotor filled with water. The rotor volume was reduced by Teflon inserts. The drawing is made at scale. (B) two-dimensional projection image of the phantom object obtained with the sequence of Fig. 2B. The MAS frequency was set to 30.03 Hz. The spectral width was 400 kHz in both dimension. A radiofrequency (rf) field strength of 167 kHz was used (90° pulse of 1.5 μ s). Detection was started on the top of the echo, using an echo time of $t_e = 10 \mu$ s. Eight scans were accumulated for each of the 64 complex points in t_1 . Quadrature detection in t_1 was performed using the States [23] method. As this object is radially symmetric, the same image is obtained independent of the delay Δ , e.g., the absolute orientation of the gradient with respect to the sample. The delay between scans was 1 s. The projection was obtained in 18 min.

Fig. 3B shows the results of the MAS-STRAFI technique applied to a phantom composed of a small plastic cylinder placed in a 4 mm rotor filled with water (see Fig. 3A). All experiments were performed on a 500 MHz (11.75 T, ultra shield magnet) Bruker Avance NMR spectrometer equipped with standard Bruker 4 and 7 mm CP/MAS probeheads. The sample rotation at the magic angle was stabilized with either the standard Bruker spinning controller (used with the 7 mm probehead) or the Bruker RockSolid stabilizer allowing stabilization at very low spinning speeds (used with the 4 mm probehead). In all experiments, the probehead was set 7 cm below its standard position in the magnet, leading to a proton spectrum (profile) of 80–100 kHz width due to the gradient of the stray field.

Fig. 3B shows a two-dimensional projection image of the phantom object obtained using the pulse sequence of Fig. 2B. The signal comes from the water surrounding the object, which itself appears black in the image. The geometry of the sample given in Fig. 3A is well reproduced in the MAS-STRAFI image, with water signal appearing inside and outside the plastic cylinder, as well as in the empty space inside the cap and the inserts of the rotor. Due to the perfect symmetry of the sample with respect to the rotor axis, rotation of the projection plane by changing the delay Δ between the synchronization pulse and the initial excitation pulse lead to identical images.

The slight distortions visible in the image, e.g., the apparent non-parallel walls of the cylinder, arise essentially from two sources. One source of image distortion comes from the motion of the rotor during each t_1 , t_2 , or t_3 window. Most simply, the rotor should hop instantaneously between 120° steps and stop during the various acquisition dimensions, such that the different acquisition times t_1 , t_2 , and t_3 are performed at precise positions of the rotor. The first solution to reduce the image distortions coming from the constant rotation of the sample is to spin as slow as possible, thereby limiting the change in the gradient orientation during the various acquisition times. It is to note that the possibility to reduce the spinning speed is limited by the relaxation time T_2 of the signal. In the projection of Fig. 3B, maximum changes of 1.7° ($t_{1,\max} = 158,5 \mu\text{s}$) and 7.5° ($t_{2,\max} = 690 \mu\text{s}$) in the gradient orientation have to be considered during the indirect and direct detection times, respectively. This small rotation of the object during the incremented acquisition times corresponds to a non-linear sampling of the k -space, resulting in distortions of the image when the points are linearly represented, as is the case in Fig. 3B. However this kind of distortions can be numerically corrected by calculating the real sampling of the k -space corresponding to the experimental parameters used, and eventually linearized the sampling through interpolation of the points. It is to note that errors in effective gradient direction due to the

rotation of the rotor during acquisition times are reduced if the acquisition times are incremented symmetrically with respect to the ideal position of the rotor. This is done by moving both the pulses before and after each of the t_n evolution periods by half of the acquisition increment in opposite directions. This insures that the acquisition windows spend equal time on either side of the idealized 120° hop positions (labeled G_x , G_y , or G_z in Fig. 2).

A second source of image distortion results from a non-linear magnetic field across the sample region (non-constant gradient). Indeed, being limited in radio-frequency (rf) field strength, we choose the position in the stray field such that the proton spectrum could still be entirely excited by a single pulse, and did not optimize for a region of the magnet with constant z -gradient and negligible radial variations [7,12]. To solve this problem, the gradient itself could be mapped, and the map used to correct the image. This source of distortions becomes less important when the sample size is made smaller.

A final image distortion problem can occur due to the echo detection in the z -filtered experiments. If the echo time (t_e in Fig. 2) is set to exactly one rotor period, then no distortion is introduced, but at slow spinning speeds, such a long echo time will result in substantial signal loss. If a short echo time is used instead, the observed stimulated echo may not refocus completely since the two t_e periods have slightly different gradient orientations over each t_e period. The solution of using a very short t_e and combine it with very slow spinning seems to fix most of the problems associated with this echo difference. Alternatively, the refocusing pulse for echo detection could be completely eliminated if the dead time of the probehead is sufficiently short.

Results obtained from a green coffee bean are given in Fig. 4. The signal arises primarily from the oils and residual water in the bean. As the coffee bean is not radially symmetric, projections around different axis can be obtained by changing the delay Δ . The rotation of the projection plane in the series of images is noticeable from the localization of the bean groove, which is visible in several projections and indicated with a white arrow. The coffee bean was slightly too thick to be put in a 7 mm rotor, and had therefore to be slightly cut on two sides. This explains the rectangular shape of the projections with $\Delta = 0.4$ and 0.6 ms, where the projection plane probably lies close to the rotor axis.

One of the major difficulties with the MAS-STRAFI experiment is the requirement for high power broadband rf excitation. Indeed, all pulses have to be short enough to excite the whole proton frequency range. As our probeheads are limited in rf-power, we could not use a higher stray field gradient, than the one found 7 cm below the homogeneous field region in the magnet center. However, high rf-power probeheads were already re-

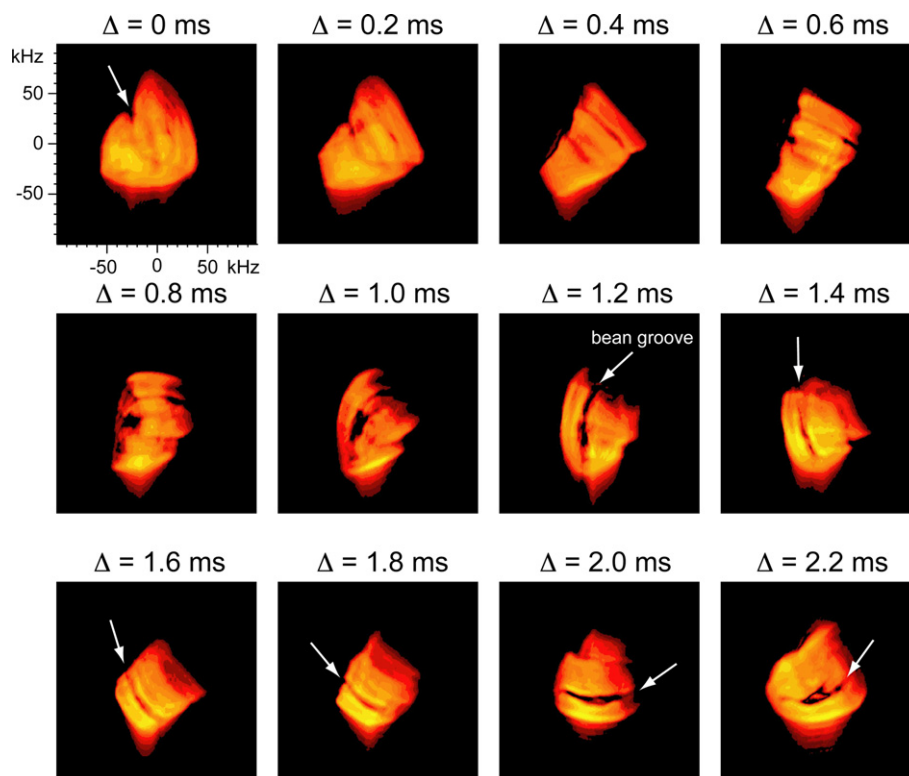


Fig. 4. Two-dimensional projection images of a green coffee bean (prior to roasting) obtained with sequence 2B. Incrementing the delay Δ in steps of 0.2 ms, corresponds to a rotation of the projection plane of 28.65° between the images. For all images, the MAS frequency was set to 400 Hz. The spectral width was 400 kHz in both dimensions and the rf field strength was $\nu_1 = 125$ kHz (90° pulse of $2 \mu\text{s}$). The echo time t_e was set to one rotor period and the full echo signal was detected. Sixteen scans were accumulated for each of the 64 complex points in t_1 . Quadrature detection in t_1 was performed using the States method [23]. The delay between scans was 2s. Each image was obtained in ~ 1 h.

quired for other applications like multiple-quantum MAS. It should be technically no problem to develop high proton rf-power MAS probe for STRAFI applications.

3. Conclusion

In conclusion, we have demonstrated that the combination of STRAFI and MAS can successfully be used to obtain high-resolution multi-dimensional images of small objects. At this point the method has not been refined enough to deliver quantitative data as density differences, or physical dimensions, about the structure of the sample, but we anticipate that this new technique will yield valuable microscopic information from a wide range of materials as further advances are made in this area. Given the enormous range of MRI experiments developed since the advent of the early image reconstruction algorithms, we optimistically hope that new pulse sequences might be developed to improve both signal-to-noise as well as resolution in this experiment. Finally, it may be that a probe specifically designed for imaging small objects in this manner with a micro coil will give substantial improvement in the

overall effectiveness and usefulness of this method. Also, it may be feasible that strongly dipolar coupled solids might be studied using this kind of approach where the homogenous linewidth is too large to provide adequate resolution with lower pulsed gradient methods. The gradient reorientation technique using MAS could be extended to other gradient sources, allowing three-dimensional images in an external inhomogeneous field, in analogy to recently proposed *ex situ* NMR spectroscopy [22].

References

- [1] P.C. Lauterbur, Image formation by induced local interactions, *Nature* 242 (1973) 190–191.
- [2] P. Mansfield, P.K. Grannell, NMR diffraction in solids, *Journal of Physics C: Solid State Physics* 6 (1973) L422–L426.
- [3] P.T. Callaghan, J. Stepisnik, Spatially distributed pulsed gradient spin echo NMR using single-wire proximity, *Physical Review Letters* 75 (1995) 4532–4535.
- [4] A.A. Samoilenko, D.Y. Artemov, L.A. Sibeldina, Formation of sensitive layer in experiments on NMR subsurface imaging of solids, *JETP Letters* 47 (1988) 417–419.
- [5] T.B. Benson, P.J. McDonald, Profile amplitude-modulation in stray field magnetic resonance imaging, *Journal of Magnetic Resonance Series a* 112 (1995) 17–23.

- [6] P.J. McDonald, Stray field magnetic resonance imaging, *Progress in Nuclear Magnetic Resonance Spectroscopy* 30 (1997) 69–99.
- [7] P.J. McDonald, B. Newling, Stray field magnetic resonance imaging, *Reports on Progress in Physics* 61 (1998) 1441–1493.
- [8] M.J.D. Mallett, M.R. Halse, J.H. Strange, Stray field imaging by magnetic field sweep, *Journal of Magnetic Resonance* 132 (1998) 172–175.
- [9] J. Godward, E. Ciampi, M. Cifelli, P.J. McDonald, Multidimensional imaging using combined stray field and pulsed gradients, *Journal of Magnetic Resonance* 155 (2002) 92–99.
- [10] B.A.M. GmbH, in UK Patent Application (GB, 1993)..
- [11] A.A. Samoilenko, K. Zick, Stray field imaging (STRAFI) advances, *Bruker Report* 1 (1990) 40–41.
- [12] J.H. Iwamiya, S.W. Sinton, Stray field magnetic resonance imaging of solid materials, *Solid State Nuclear Magnetic Resonance* 6 (1996) 333–345.
- [13] M.A. Baumann, G.M. Doll, K. Zick, Stray field imaging (STRAFI) of teeth, *Oral Surgery Oral Medicine Oral Pathology Oral Radiology and Endodontics* 75 (1993) 517–522.
- [14] P.S. Wang, D.B. Minor, S.G. Malghan, Binder distribution in Si_3N_4 ceramic green bodies studied by stray field NMR imaging, *Journal of Materials Science* 28 (1993) 4940–4943.
- [15] E.R. Andrew, A. Bradbury, R.G. Eades, Removal of dipolar broadening of nuclear magnetic resonance spectra of solids by specimen rotation, *Nature* 183 (1959) 1802–1803.
- [16] I.J. Lowe, Free induction decays of rotating solids, *Physical Review Letters* 2 (1959) 285–287.
- [17] A. Bax, N.M. Szeverenyi, G.E. Maciel, Correlation of isotropic shifts and chemical shift anisotropies by two-dimensional fourier-transform magic-angle hopping NMR spectroscopy, *Journal of Magnetic Resonance* 52 (1983) 147–152.
- [18] J.Z. Hu, A.M. Orendt, D.W. Alderman, C.H. Ye, Improvements to the magic-angle hopping experiment, *Solid State Nuclear Magnetic Resonance* 2 (1993) 235–243.
- [19] Z. Gan, High-resolution chemical shift and chemical shift anisotropy correlation in solids using slow magic angle spinning, *Journal of the American Chemical Society* 114 (1992) 8307–8309.
- [20] S.L. Gann, J.H. Baltisberger, A. Pines, Dynamic-angle spinning without sidebands, *Chemical Physics Letters* 210 (1993) 405–410.
- [21] J.Z. Hu, D.W. Alderman, C.H. Ye, R.J. Pugmire, D.M. Grant, An isotropic chemical shift-chemical shift anisotropy magic-angle slow-spinning 2D NMR experiment, *Journal of Magnetic Resonance* 105 (1993) 82–87.
- [22] C.A. Meriles, D. Sakellariou, H. Heise, A.J. Moule, A. Pines, Approach to high-resolution ex situ NMR spectroscopy, *Science* 293 (2001) 82–85.
- [23] D.J. States, R.A. Haberkorn, D.J. Ruben, A two-dimensional nuclear Overhauser experiment with pure absorption phase in four quadrants, *Journal of Magnetic Resonance* 48 (1982) 286–292.